RESEARCH ARTICLE

SRSF1 regulates primordial follicle formation and number determination during meiotic prophase I

Longjie Sun[1†], Zheng Lv[1†], Xuexue Chen[1], Chaofan Wang[1], Pengbo Lv[1], Lu Yan[1], Shuang Tian[1], Xiaomei Xie[1], Xiaohong Yao[1], Jingjing Liu[1], Zhao Wang[1], Haoshu Luo[1], Sheng Cui[2] and Jiali Liu[1*]

Abstract

Background Ovarian folliculogenesis is a tightly regulated process leading to the formation of functional oocytes and involving successive quality control mechanisms that monitor chromosomal DNA integrity and meiotic recombination. A number of factors and mechanisms have been suggested to be involved in folliculogenesis and associated with premature ovarian insufficiency, including abnormal alternative splicing (AS) of pre-mRNAs. Serine/arginine-rich splicing factor 1 (SRSF1; previously SF2/ASF) is a pivotal posttranscriptional regulator of gene expression in various biological processes. However, the physiological roles and mechanism of SRSF1 action in mouse early-stage oocytes remain elusive. Here, we show that SRSF1 is essential for primordial follicle formation and number determination during meiotic prophase I.

Results The conditional knockout (cKO) of *Srsf1* in mouse oocytes impairs primordial follicle formation and leads to primary ovarian insufficiency (POI). Oocyte-specific genes that regulate primordial follicle formation (e.g., *Lhx8*, *Nobox*, *Sohlh1*, *Sohlh2*, *Figla*, *Kit*, *Jag1*, and *Rac1*) are suppressed in newborn *Stra8-GFPCre Srsf1*[Fl/Fl] mouse ovaries. However, meiotic defects are the leading cause of abnormal primordial follicle formation. Immunofluorescence analyses suggest that failed synapsis and an inability to undergo recombination result in fewer homologous DNA crossovers (COs) in the *Srsf1* cKO mouse ovaries. Moreover, SRSF1 directly binds and regulates the expression of the POI-related genes *Six6os1* and *Msh5* via AS to implement the meiotic prophase I program.

Conclusions Altogether, our data reveal the critical role of an SRSF1-mediated posttranscriptional regulatory mechanism in the mouse oocyte meiotic prophase I program, providing a framework to elucidate the molecular mechanisms of the posttranscriptional network underlying primordial follicle formation.

Keywords SRSF1, Alternative splicing, Oocyte, Meiosis, Primary ovarian insufficiency

†Longjie Sun and Zheng Lv contributed equally to this work.

*Correspondence:
Jiali Liu
liujiali@cau.edu.cn
[1] State Key Laboratory of Farm Animal Biotech Breeding, College of Biological Sciences, China Agricultural University, Beijing 100193, China
[2] College of Veterinary Medicine, Yangzhou University, Yangzhou, Jiangsu 225009, China

Background

High-quality gametes are critical for successful reproduction [1]. Functional oocytes are derived from successful folliculogenesis in the ovaries, which includes primordial follicle formation; recruitment into the growing pool to form primary, secondary, and tertiary follicles; ovulation; and subsequent corpus luteum formation [2]. The size and quality of the surviving pool of primordial follicles are essential determinants of female fecundity and reproductive lifespan [3]. To maintain quality, diverse

Sun *et al. BMC Biology*   (2023) 21:49

Page 2 of 18

organisms have evolved three quality control mechanisms for eliminating meiocytes with defects in meiotic recombination or SPO11-linked DNA double-strand break (DSB) accumulation, namely, meiotic silencing, the synapsis checkpoint, and the DNA damage checkpoint [4]. During meiotic prophase I, defective meiosis results in POI due to early exhaustion of the follicle pool.

With the widespread application of next-generation sequencing (NGS), the genetic spectrum of POI has been expanded, especially by the recent identification of novel meiosis-related genes [5–7]. The cohesin complex regulates sister chromatid cohesion and synaptonemal complex (SC) formation and is composed of the meiosis-specific subunits STAG3, RAD21L, and SMC1β and the nonspecific subunits SMC3 and REC8 [8]. STAG3 aberrations have been identified to cause a rare monogenic type of POI [9–18]. The chromosome axis forms a platform for SC assembly, which plays a central role in homologous pairing, recombination, and chromosome segregation. The central elements of SCs include SYCE1-3, SIX6OS1, and TEX12. Mutations in SYCE1 and SIX6OS1 have been identified in POI patients [19–23]. Notably, the abnormal AS of MEIOB, STAG3, MSH4, and MCM9 pre-mRNAs has been observed in human POI [15, 24–26]. However, the mechanisms that regulate pre-mRNA splicing during the progression of meiotic prophase I in mouse oocytes are poorly understood.

SRSF1 is a pivotal posttranscriptional regulator of gene expression in various biological processes [27, 28]. Unfortunately, homozygous *Srsf1* knockout mice exhibit early embryonic lethality [29]. Therefore, conditional *Srsf1* deletion mouse models have been applied in studies of its role in the heart and thymus [29–33]. Interestingly, single-cell RNA sequencing has demonstrated that the expression of SRSF1 first decreases and then increases during the oocyte meiotic prophase I program [34]. However, the physiological roles of SRSF1 during oocyte meiotic prophase I are still largely unclear. This study shows that conditional knockout of *Srsf1* in mouse oocytes impairs primordial follicle formation and leads to POI. We further verified that SRSF1 directly binds and regulates *Six6os1* and *Msh5* expression via AS, which is critical for implementing the meiotic prophase I program.

Results

SRSF1 deficiency leads to premature ovarian insufficiency

The results of SRSF1 and VASA co-staining revealed that SRSF1 was expressed in the nuclei of oocytes and granulosa cells of the adult mouse ovary. Intriguingly, SRSF1 was highly expressed in the nucleus of the primordial follicle oocyte (Fig. 1a − f). To investigate the role of SRSF1 in POI, the expression pattern of SRSF1 during ovarian development and ageing was evaluated. Intriguingly,

SRSF1 expression was reduced in the primordial follicle oocytes of ageing ovaries (Additional file 1: Fig. S1). These data suggest that SRSF1 may contribute to physiological ovarian ageing. To further study the detailed expression pattern of SRSF1 in primordial follicle formation, we observed oocytes at different meiotic stages in mouse ovaries by co-immunostaining with antibodies against SRSF1 and synaptonemal complex protein 3 (SYCP3). Interestingly, SRSF1 expression was high in leptotene spermatocytes and further increased in pachytene spermatocytes (Fig. 1g − k), suggesting that SRSF1 plays an essential role in forming primordial follicles.

To define the specific involvement of SRSF1 in primordial follicle formation, we studied the physiological roles of SRSF1 in vivo using a mouse model. Considering that global SRSF1 knockout is lethal in mice [29], we used *Srsf1* cKO mice in which *Srsf1* is deleted at the time of meiosis initiation, starting at 12.5 days post-coitus (dpc), by the *Stra8-GFPCre* transgene [35, 36] (Fig. 2a, b). We used a conditional allele of *Srsf1* (*Srsf1*^{Fl}) in which exons 2, 3, and 4 of *Srsf1* are flanked by two *loxP* sites (Fig. 2a). By crossing *Srsf1*^{Fl} and *Stra8-GFPCre* mice, we obtained *Stra8-GFPCre Srsf1*^{Fl/Fl} mice with *Srsf1* deletion in oocytes (Fig. 2a, c). We verified the absence of the SRSF1 protein in all postnatal oocytes by co-immunofluorescence analysis with SRSF1 and VASA antibodies (Fig. 2d − g).

The adult cKO mice were normal in size (Fig. 2h, i), but the size of their ovaries was significantly reduced (Fig. 2j, k). To further confirm the effect of the loss of *Srsf1* on female fertility, a breeding experiment was performed, and the data indicated that the absence of *Srsf1* led to complete infertility in cKO females (Fig. 2l). Histological examination of cKO ovary sections revealed that folliculogenesis was arrested (Fig. 2m − p). Immunostaining of VASA indicated the absence or asymmetric deviation of oocytes in cKO ovaries (Fig. 2q − t). Follicle count data based on VASA immunohistochemistry analysis showed that the follicles in cKO ovaries were primarily arrested at the primary follicle stage (Fig. 2u, v). Together, these results indicate that SRSF1 is critical for follicle development.

SRSF1 is required for mouse primordial follicle formation

To confirm the effect of the loss of *Srsf1* on POI, we examined mouse ovaries at 5 days post-partum (dpp), a timepoint at which the primordial follicle pool is successfully established [34]. Tissue analyses revealed that the cKO mice exhibited a reduced ovary size (Fig. 3a, b). Oocyte count data based on VASA immunohistochemistry analysis showed that the primordial follicle pool was consistently reduced in cKO ovaries (Fig. 3e). We verified that the numbers of naked oocytes or oocytes in the
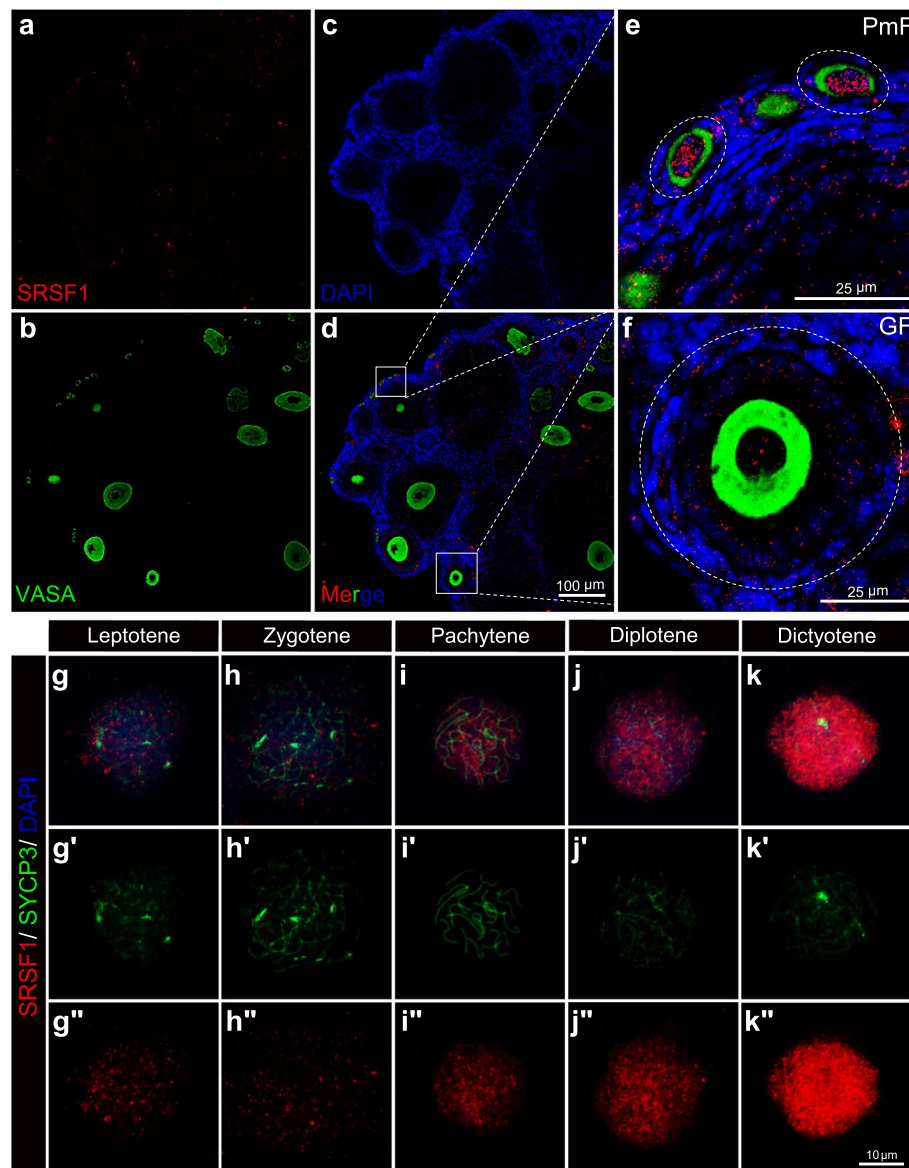
Sun *et al. BMC Biology*   (2023) 21:49

Page 3 of 18

Fig. 1 Dynamic localization of SRSF1 in mouse oocytes. **a–f** SRSF1 is highly expressed in oocytes of the primordial follicle. Immunostaining was performed using VASA and SRSF1 antibodies from adult mouse ovaries. DNA was stained with DAPI. **a–d** Scale bar, 100 μm. The **e** primordial follicle (PmF) and **f** grown follicle (GF) are shown in the magnified views. Scale bar, 25 μm. **g–k** The dynamic localization of SRSF1 to the oocyte meiotic prophase I program. Co-immunostaining was performed using SYCP3 and SRSF1 antibodies from 15.5 dpc, 17.5 dpc, 18.5 dpc, and 1 dpp oocyte surface spreading. DNA was stained with DAPI. **g′–k′** The meiotic stages of the oocytes were determined by SYCP3 staining (green). **g″–k″** The dynamic localization of SRSF1(red) during the oocyte meiotic prophase I program. Scale bar, 10 μm

cysts were increased, but the numbers of primordial and primary follicles were reduced, in cKO ovaries (Fig. 3c, d, f). Together, these results suggest dysfunctional primordial follicle formation and number determination in cKO ovaries.

The specific involvement of SRSF1 in primordial follicle formation and number determination was further verified by the observation of mild ovarian atrophy in newborn cKO mice, in which the primordial follicle pool is being established (Fig. 3g, h). RT–qPCR showed that the expression of *Srsf1* was significantly decreased in cKO ovaries (Fig. 3m), and co-immunofluorescence analysis with SRSF1 and VASA antibodies showed an absence of the SRSF1 protein in all oocytes (Fig. 2d − g). Interestingly, VASA immunostaining revealed more oocytes in cysts in cKO ovaries (Fig. 3i − l). RT–qPCR results showed that the expression of *Vasa* was significantly decreased in the cKO ovaries, suggesting that the

Sun *et al. BMC Biology*   (2023) 21:49

Page 4 of 18

total number of oocytes was reduced (Fig. 3n). Additionally, count data showed that the numbers of both total oocytes and primary follicles were reduced in cKO ovaries (Fig. 3o, p). However, the number of oocytes in cysts was significantly increased (Fig. 3p). Abnormal primordial follicular pool formation was further confirmed by the observation of GM130 immunofluorescence in the ovaries of newborn cKO mice [37]. Our results revealed that the number of double-positive cells was reduced in newborn cKO ovaries, suggesting that SRSF1 is essential for cyst breakdown and primordial follicle formation (Fig. 3q, r). To understand the molecular mechanisms underlying these phenotypes, we examined vital genes that regulate primordial follicle formation by RT–qPCR and found that their expression was suppressed (Fig. 3s). Co-immunostaining of VASA and KIT or JAG1 showed that the number of double-positive cells was reduced in the ovaries of newborn cKO mice (Fig. 3t − w). These data suggest that vital genes that regulate primordial follicle formation are suppressed in the ovaries of newborn cKO mice.

Loss of SRSF1 impairs meiotic progression in oocytes

To investigate the molecular consequences of SRSF1 depletion in primordial follicle formation, we isolated mRNA from control (Ctrl) and cKO ovaries at 16.5 dpc and performed RNA sequencing. RNA-seq analyses identified 566 downregulated and 705 upregulated genes in cKO ovaries at 16.5 dpc (Fig. 4a, b; Additional file 2: Table 1). Surprisingly, Gene Ontology (GO) term enrichment indicated abnormal meiosis in cKO mouse oocytes (Fig. 4c). Next, we validated the abnormal expression of meiosis-related genes (downregulated: *Rec8*, *Six6os1*, *Psmc3ip*, *Tdrd9*, and *Plk1*; upregulated: *Hormad2* and *Syce1*) by RT–qPCR (Fig. 4d). To assess meiotic progression in cKO ovaries, MSY2 immunostaining was employed as a marker of the diplotene stage in newborn

mouse ovaries (Fig. 4e) [38]. Double-positive cell counting results showed that the number of diplotene oocytes was reduced in cKO ovaries (Fig. 4f). To further evaluate this phenotype, we performed SYCP3 immunofluorescence analysis in 5 dpp mouse ovaries (Fig. 4g). Normal meiotic arrest in the dictyate stage is crucial for primordial follicle formation. It can be identified by the presence of two to four visible nucleolus signals after staining with an SYCP3 antibody [39]. Dictyate oocyte count data revealed that SRSF1 deficiency impaired meiotic progression to the diplotene stage in oocytes (Fig. 4h). These results suggest that the few oocytes in cKO ovaries that reached the diplotene stage could not develop further to the dictyate stage.

SRSF1 deficiency leads to defects in synapsis and crossover recombination in cKO ovaries

The GO term enrichment results showed abnormal homologous chromosome segregation in cKO mouse oocytes (Fig. 4c). The COs cause the exchange of homologous DNA and establish the physical connections between homologues required for proper chromosome segregation [40]. MutL homologue 1 (MLH1) has been recognized as a classic marker of COs [41–43]. Therefore, the distribution of MLH1 foci was evaluated by MLH1 and SYCP3 immunostaining in newborn mouse oocyte surface spreads (Fig. 5a). The counts of MLH1 foci showed that the formation of COs was reduced in diplotene oocytes (Fig. 5b). The final and significant purpose of meiotic recombination is the formation of COs [44, 45]. To probe the nature of meiotic recombination in cKO ovaries, we examined chromosomal synapsis through oocyte surface spread analysis in newborn mouse ovaries. Aberrant synapsis was frequently observed in cKO oocytes based on the localization of synaptonemal complex protein 1 (SYCP1), SYCP3, and CREST (Fig. 5c). Surprisingly,

(See figure on next page.)

Fig. 2 SRSF1 plays critical roles in follicle development and female fertility. **a** *Stra8-GFPCre* mice were crossed with *Srsf1^Fl/Fl^* mice to generate *Srsf1* cKO mice. Cre-mediated deletion removed exons 2, 3, and 4 of *Srsf1* and generated a null protein allele. **b** Schematic diagram of Cre enzyme expression showing the spatiotemporal patterns of major cellular events in mouse early phase ovaries. **c** Genotyping PCRs were performed using *Stra8-GFPCre* and *Srsf1* primers. **d–g** Co-immunostaining of SRSF1 and VASA in adult Ctrl and cKO ovaries. PmF, primordial follicle; PF, primary follicle. Scale bar, 25 μm. **h, i** Normal body weight in cKO mice. The body sizes and weights of adult Ctrl and cKO mice are shown as the mean ± SEM. *n* = 5. **j, k** Ovarian atrophy in adult cKO mice. Ovary sizes and weights of adult Ctrl and cKO mice are shown as the mean ± SEM. *n* = 5. **i** Fertility test results showing an infertility phenotype in the cKO females (*n* = 8) compared to that in the Ctrl mice (*n* = 6) during 180 days of mating. **m–p** Haematoxylin stained ovary sections from adult Ctrl and cKO mice are shown. **m, n** Scale bar, 500 μm. **o, p** Magnified views are shown. Scale bar, 50 μm. **q–t** Immunostaining of VASA in adult Ctrl and cKO ovaries. DNA was stained with DAPI. Red arrows indicate abnormal follicles of oocytes deviating to one side. Red arrowheads indicate oocyte-free follicles. Scale bar, 50 μm. **u, v** Folliculogenesis was arrested in the cKO ovaries. **u** Immunostaining of VASA in adult Ctrl and cKO ovaries. DNA was stained with haematoxylin. PmF, primordial follicle; Scale bar, 20 μm. PF, primary follicle; SF, secondary follicle; AF, antral follicle; CL, corpus luteum; Scale bar, 100 μm. **v** Counting of the significant mouse stages of folliculogenesis. *n* = 4. Significance was determined by unpaired Student's *t* test; detailed *P* value *P* ≥ 0.05, **P* < 0.05, ****P* < 0.001, *****P* < 0.0001. The error bar represents the mean ± SEM
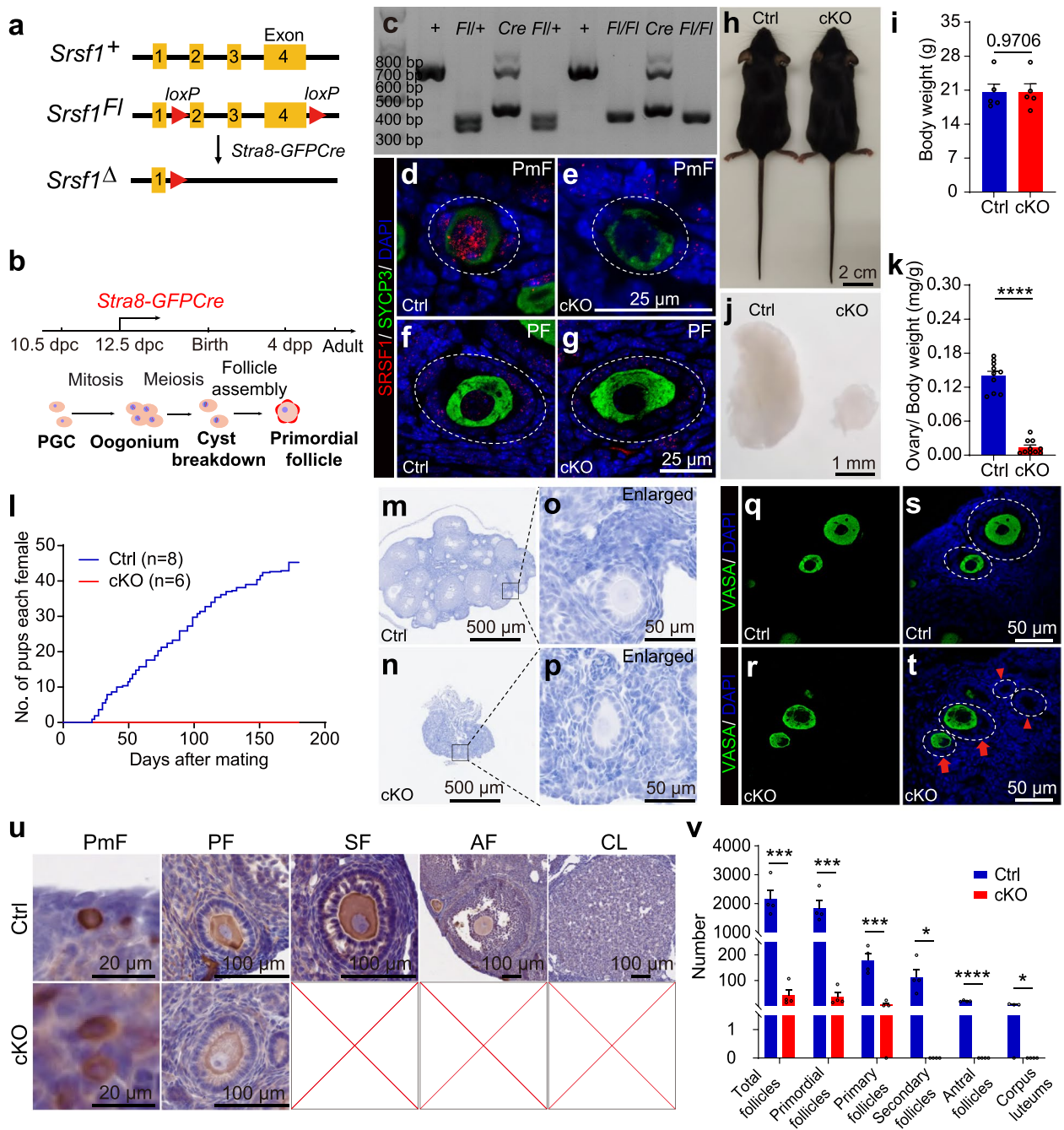
Fig. 2 (See legend on previous page.)

SYCP1 could not be loaded onto chromosomes in cKO mouse oocytes (Fig. 5c). The provided schematic diagram shows the failure of synapsis in cKO oocytes (Fig. 5d, e). These data suggest that the failure of synapsis and the inability to undergo homologous recombination (HR) resulted in fewer COs in cKO oocytes.

SRSF1 is essential for the resection of SPO11-linked DNA double-strand breaks (DSBs)

DSBs formed during meiosis recruit phosphorylated histone H2AX (γH2AX) [46]. Therefore, we monitored the progression of meiotic recombination in 17.5 dpc ovaries by the co-immunostaining with γH2AX and SYCP3. The immunostaining results revealed distinct γH2AX signals

Sun *et al. BMC Biology*   (2023) 21:49

Page 6 of 18

in cKO oocytes, whereas few oocytes in Ctrl ovaries showed positive γH2AX staining (Fig. 6a). The double-positive cell counting data confirmed that some DSBs were not repaired correctly in cKO oocytes (Fig. 6b). Replication protein A (RPA) is a single-strand DNA-binding heterotrimeric complex composed of RPA1, RPA2, and RPA3 that is essential for meiotic recombination [47]. We examined the localization of RPA1 as a representative of the RPA complex by nuclear spread analysis in newborn mouse ovaries. The co-immunostaining of RPA1 and SYCP3 showed that many RPA complexes remained uncleared in the diplotene stage in cKO oocytes (Fig. 6c, d). RecA-like proteins DMC1 and RAD51 form a nucleoprotein filament on ssDNA within DSBs to aid in the search and invasion of the homologous partner for successful recombination and synapsis. We further explored the distribution of proteins involved in recombination and DSB repair. Interestingly, the localization of DMC1, γH2AX, and SYCP3 showed that significant DMC1 foci were present on chromosomes in the pachytene stage in cKO oocytes (Fig. 6e). The DMC1 focus count data revealed an increase in recombinase on chromosomes in the pachytene stage in cKO oocytes (Fig. 6f). However, the recombinase had lost its ability to effect on DNA repair. These observations suggest that SRSF1 is essential for the resection of SPO11-linked DSBs in meiotic prophase.

SRSF1 directly regulates the splicing of the POI-related genes *Msh5* and *Six6os1*

RNA-seq analyses showed 191 AS events that were identified as significantly affected (FDR < 0.05) in 16.5 dpc cKO ovaries (Additional file 3: Table 2). Among the 191 affected AS events, most (141) were classified as skipped exons (SEs). In addition, ten AS events were categorized as alternative 5′ splice sites (A5SSs), 10 as alternative 3′ splice sites (A3SSs), 15 as mutually exclusive exons (MXEs), and 15 as retained introns (RIs) (Fig. 7a). The GO enrichment analysis of the alternatively spliced genes revealed that eleven meiosis-related genes showed alterations in AS forms (Fig. 7b). At least two (*Six6os1* and *Msh5*) of these genes have been associated with POI [19, 20, 48]. We then visualized the different types of AS based on RNA-seq data by using Integrative Genomics Viewer (IGV, 2.10.2) software (Fig. 7c). RT–PCR results showed that the pre-mRNAs of *Six6os1* and *Msh5* in cKO mouse oocytes exhibited abnormal AS (Fig. 7d). The results of RIP–qPCR showed that SRSF1 could bind to the pre-mRNAs of *Msh5* and *Six6os1* (Fig. 7e, f). Interestingly, Western blotting and immunostaining revealed that the protein levels of MSH5 and SIX6OS1 were significantly suppressed (Fig. 7g − k; Additional file 4: Fig. S2a, b). Additionally, abnormal AS changed the mRNA decay rates of *Six6os1* (Fig. 7l) but not *Msh5* (Additional file 4: Fig. S2c) in cKO mouse ovaries.

Discussion

Abnormal follicle stock formation induces POI

The primordial follicle pool that forms perinatally is a female's sole lifelong source of oocytes [49]. POI is determined by the exhaustion of the primordial follicle pool in the ovaries [5]. In cKO ovaries, we found more oocytes in cysts but a reduced number of total oocytes and primordial follicles. Our data suggest that cyst breakdown and primordial follicle formation are disrupted in cKO oocytes. Similar phenotypes have been observed following the loss of oocyte-specific genes (e.g., *Lhx8*, *Nobox*, *Sohlh1*, *Sohlh2*, *Figla*, *Kit*, *Jag1*, and *Rac1*) [50–56]. This study showed that most oocyte-enriched genes that regulate primordial follicle formation are suppressed in the ovaries of newborn cKO mice (Fig. 3s; Additional file 5: Fig. S3).

Interestingly, although the level of JAG1 protein was significantly reduced (Fig. 3v, w), there was no significant change in the *Jag1* mRNA level in the ovaries of newborn cKO mice (Fig. 3s). We speculate that SRSF1 acts as an essential splicing factor for *Jag1* and other regulatory factors involved in primordial follicle

(See figure on next page.)

Fig. 3 SRSF1 is required for mouse primordial follicle formation. **a, b** Ovarian atrophy in 5 dpp cKO mice. **c, d** Immunostaining of VASA in 5 dpp ovaries. PF, primary follicle (**c′, d′**), PmF, primordial follicle (**c″**), cyst oocytes (**d″**)**,** naked oocyte (**d‴**). **e** Quantification of total oocytes per 5 dpp ovary. **f** Quantification of primordial follicles, primary follicles, and oocytes in cysts or naked per 5 dpp ovary. *n* = 3. **g, h** Ovarian atrophy in newborn cKO mice. **i–l** Immunostaining of VASA in newborn ovaries. **k′, l′** The primordial follicle and oocytes in cysts are shown in magnified views. Arrowheads, PmF; arrows, cyst oocytes. **m** The mRNA level of *Srsf1* decreased in newborn cKO ovaries. **n** The mRNA level of *Vasa* decreased in newborn cKO ovaries. **o** Quantification of total oocytes per newborn ovary. Ctrl, *n* = 3; cKO, *n* = 4. **p** Percentages of primordial follicles and oocytes in cysts per newborn ovary. Ctrl, *n* = 3; cKO, *n* = 4. **q** Co-immunostaining of GM130 and VASA in newborn ovaries. **r** Percentage of double-positive cells in newborn ovaries. *n* = 2. **s** *Srsf1* deficiency downregulated expression of various genes (e.g., *Kit, Rac1, Figla, Nobox*). **t** Co-immunostaining of KIT and VASA in newborn ovaries. **u** Percentage of double-positive cells in newborn cKO ovaries. *n* = 3. **v** Co-immunostaining of JAG1 and VASA in newborn ovaries. **w** Percentage of double-positive cells is shown in newborn cKO ovaries. *n* = 3. Real-time qPCR data were normalized to *Gapdh* (**n, m**) or *Vasa* (**s**). *n* = 3. Significance was determined by unpaired Student's *t* test; detailed *P* value *P* ≥ 0.05, *P < 0.05, ***P < 0.001, ****P < 0.0001. The error bar represents the mean ± SEM. Scale bar, 20 μm (**q** right, **t** magnified, **v** magnified left), 50 μm (**k′, l′**), 100 μm (**c, d**), 200 μm (**a, d, i–l, q** left, **t** left, **v** left), 400 μm (**g, h**)
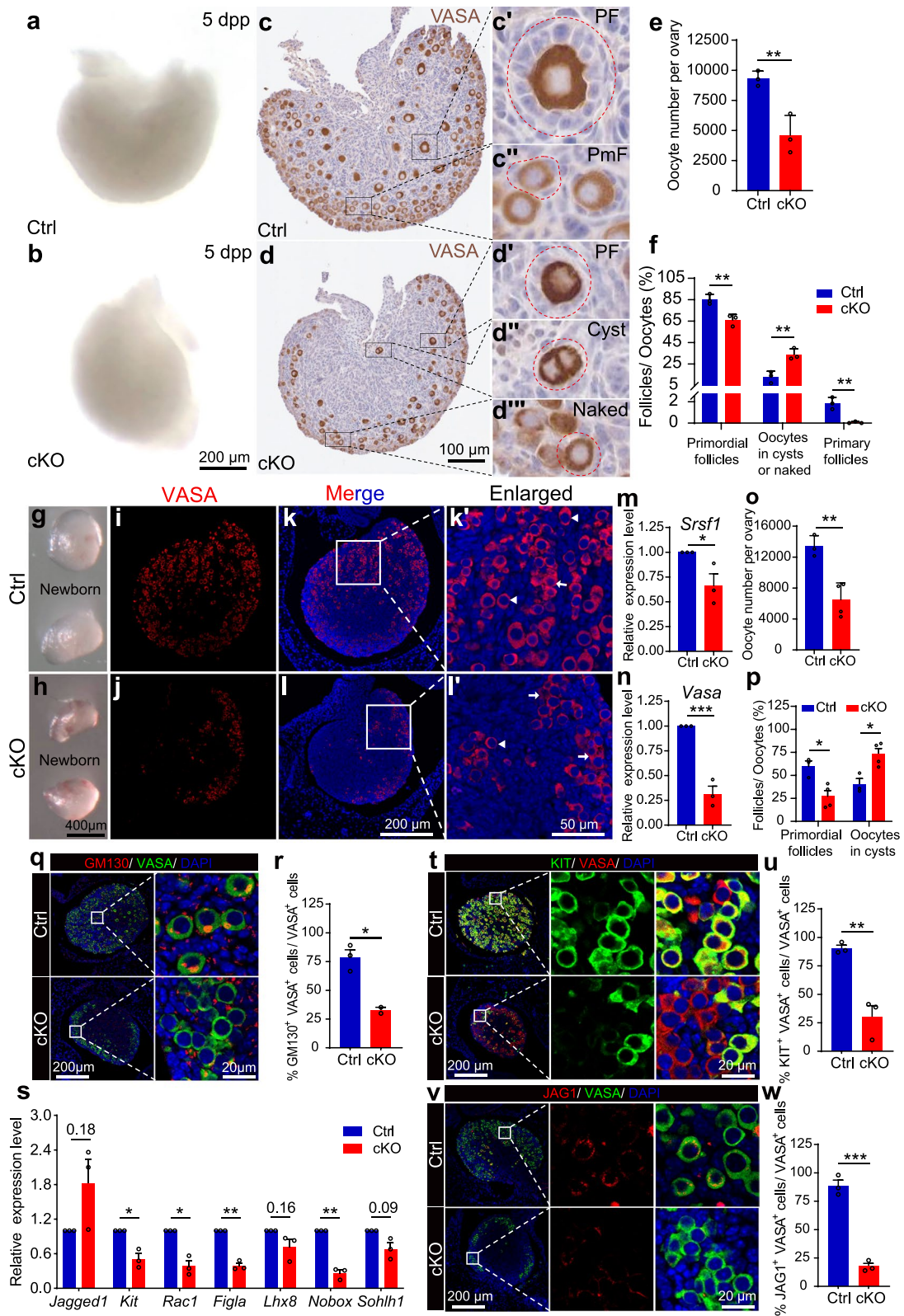
Sun *et al. BMC Biology*   (2023) 21:49

Page 7 of 18

Fig. 3 (See legend on previous page.)

Sun *et al. BMC Biology*   (2023) 21:49

Page 8 of 18

formation. However, meiotic defects are the leading cause of abnormal primordial follicle formation.

Meiotic defects impair primordial follicle formation

Routine meiotic arrest at the dictyate stage is crucial for correcting DNA damage so that sufficient follicle numbers are retained in the ovary to ensure optimal fertility for an adequate period and prevent the transmission of genetic defects to the next generation [57]. Previous studies have shown that meiosis-related genes (e.g., *Stag3*, *Syce1*, *Spidr*, *Psmc3ip*, *Hfm1*, *Msh4*, *Msh5*, *Mcm8*, *Mcm9*, *Csb-Pgbd3*, and *Nup107*) play essential roles in the assembly of primordial follicles [5]. Co-immunostaining with MSY2 and SYCP3 antibodies showed that the few oocytes that reached the diplotene stage in cKO ovaries could not develop further to the dictyate stage (Fig. 4e–h). Additionally, the abnormal expression of meiosis-related genes (e.g., *Rec8*, *Six6os1*, *Psmc3ip*, *Tdrd9*, *Plk1*, *Hormad2*, and *Syce1*) impaired oocyte meiotic progression (Fig. 4d). These results suggest that meiotic defects led to abnormal dictyate arrest during primordial follicle formation.

Abnormal AS of *Msh5* and *Six6os1* causes meiotic defects

SRSF1 directly binds and regulates interferon regulatory factor 7 (*Irf7*) and interleukin-27 receptor subunit alpha (*Il27ra*) expression via AS in the late stage of thymocyte development [30]. In addition, SRSF1 directly binds and regulates the AS of *Myb* pre-mRNA in invariant natural killer T cells. Furthermore, SRSF1 promotes cell proliferation, survival, and invasion in glioma tissues and cell lines by specifically switching the AS of myosin IB (MYO1B) [58]. Nevertheless, the physiological roles of SRSF1 during meiosis are still largely unclear. One key finding of this study is that SRSF1 directly regulates the AS of *Msh5* and *Six6os1* associated with POI during meiotic prophase I. In addition, in SRSF1-deficient oocytes, the expression of MSH5 protein levels is significantly reduced leading to POI.

MSH5 heterodimers play an essential role in the HR-based repair of DSBs [59]. Accordingly, the loss of either gene in mice results in meiotic disruption prior to the pachytene stage, including incomplete synapsis, persistence of RAD51/DMC1, and a failure to complete DSB repair [60, 61]. Unexpectedly, this study demonstrated that cKO mouse oocytes were blocked in the early diplotene stage, mainly due to the incomplete deficiency of the MSH5 protein in *Srsf1* cKO oocytes. However, we found that the number of RPA1 and DMC1 foci on chromosomes was significantly increased in *Srsf1* cKO oocytes relative to control oocytes (Fig. 6c, e) and that a large number of DSBs were not repaired correctly in *Srsf1* cKO oocytes (Fig. 6b). These phenotypes are similar to those of MSH5-deficient oocytes [61].

C14ORF39/SIX6OS1 is the central element of the SC, defects in which cause POI [20, 62]. The loss of SRSF1 leads to the abnormal splicing of *Six6os1* pre-mRNA, and SIX6OS1 does not localize to the central element of the SC in most early pachytene oocytes in this genetic background (Fig. 7k). The observed SC defects partially explain why failure of synapsis occurs in SRSF1-deficient oocytes. Synapsis provides the basis for crossover recombination [63]. Therefore, the formation of COs in diplotene oocytes is decreased (Fig. 5b). These defects prevent the diplotene oocytes from undergoing typical meiotic arrest at the dictyate stage, which seriously impairs primordial follicle formation.

Quality control mechanisms eliminate defective oocytes

Oocyte quality and number are important determinants of reproductive success [64]. The selective elimination of oocytes during the early stages of oogenesis influences these attributes and is normally observed in mammalian foetal ovaries [65]. Historically, oocyte elimination in mice has been attributed to three quality control mechanisms: meiotic silencing, the synapsis checkpoint, and the DNA damage checkpoint [4]. We observed increased DNA damage and accumulation of unrepaired DSBs, as indicated by the abundances of γH2AX and RPA1,

(See figure on next page.)

Fig. 4 SRSF1 is required for meiotic progression. **a** Volcano map displaying the distribution of differentially expressed genes from RNA-seq data. The abscissa in the figure represents the gene fold change in cKO and Ctrl mouse ovaries. |log2FoldChange|≥ 0. The ordinate indicates the significance of gene expression differences between cKO and Ctrl mouse ovaries. $P \leq 0.05$. Upregulated genes are shown in red dots, and downregulated genes are shown in green dots. **b** Cluster heatmap of differentially expressed genes. The abscissa is the genotype, and the ordinate is the normalized FPKM (fragments per kilobase million) value of the differentially expressed gene. Red indicates a higher expression level, while green indicates a lower expression level. **c** Scatter plot of GO enrichment analysis of the 1271 differentially expressed genes. The 12 most effective terms were selected to draw a scatter diagram for display. **d** The misregulation of meiosis-related genes in 16.5 dpc cKO ovaries. Real-time qPCR data were normalized to *Gapdh*. The value in newborn Ctrl ovaries was set as 1.0, and the relative value in the ovaries of newborn cKO mice is indicated. $n = 4$. **e** Co-immunostaining of MSY2 and VASA in newborn Ctrl and cKO ovaries. DNA was stained with DAPI. Scale bar, 200 μm. **f** Percentage of double-positive cells is shown as the mean ± SEM. $n = 3$. **g** Immunostaining of SYCP3 in 5 dpp Ctrl and cKO ovaries. DNA was stained with DAPI. The dictyotene oocytes of Ctrl ovaries are shown in magnified views. Abnormal oocytes of cKO ovaries are shown in the magnified views. Scale bar, 50 μm. **h** Percentage of dictyotene oocytes is shown as the mean ± SEM in 5 dpp ovaries. $n = 3$. Significance was determined by unpaired Student's *t* test; detailed *P* value $P \geq 0.05$, *$P < 0.05$, ***$P < 0.001$, ****$P < 0.0001$. The error bar represents the mean ± SEM
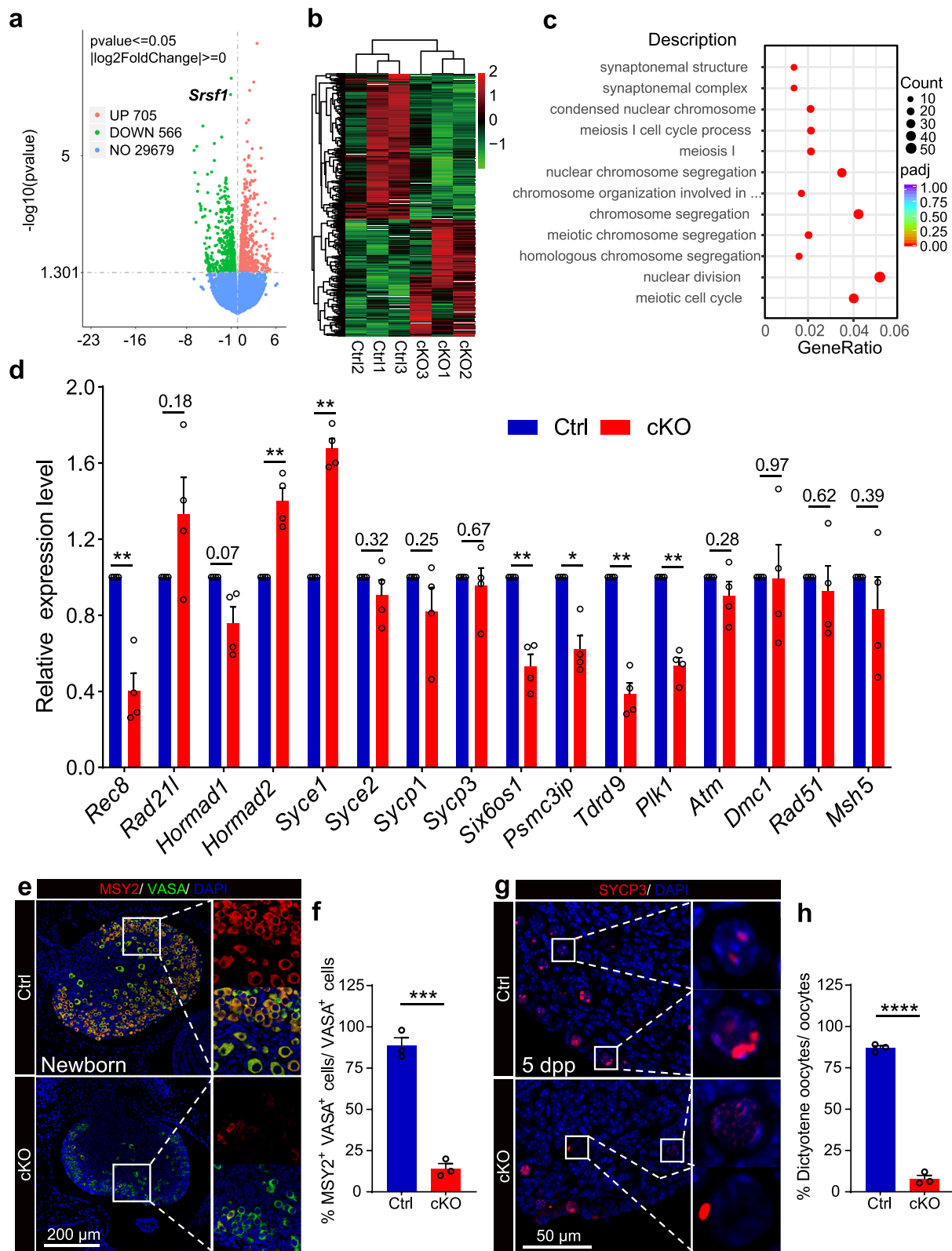
Sun *et al. BMC Biology*   (2023) 21:49

Page 9 of 18

Fig. 4 (See legend on previous page.)

Sun *et al. BMC Biology*   (2023) 21:49
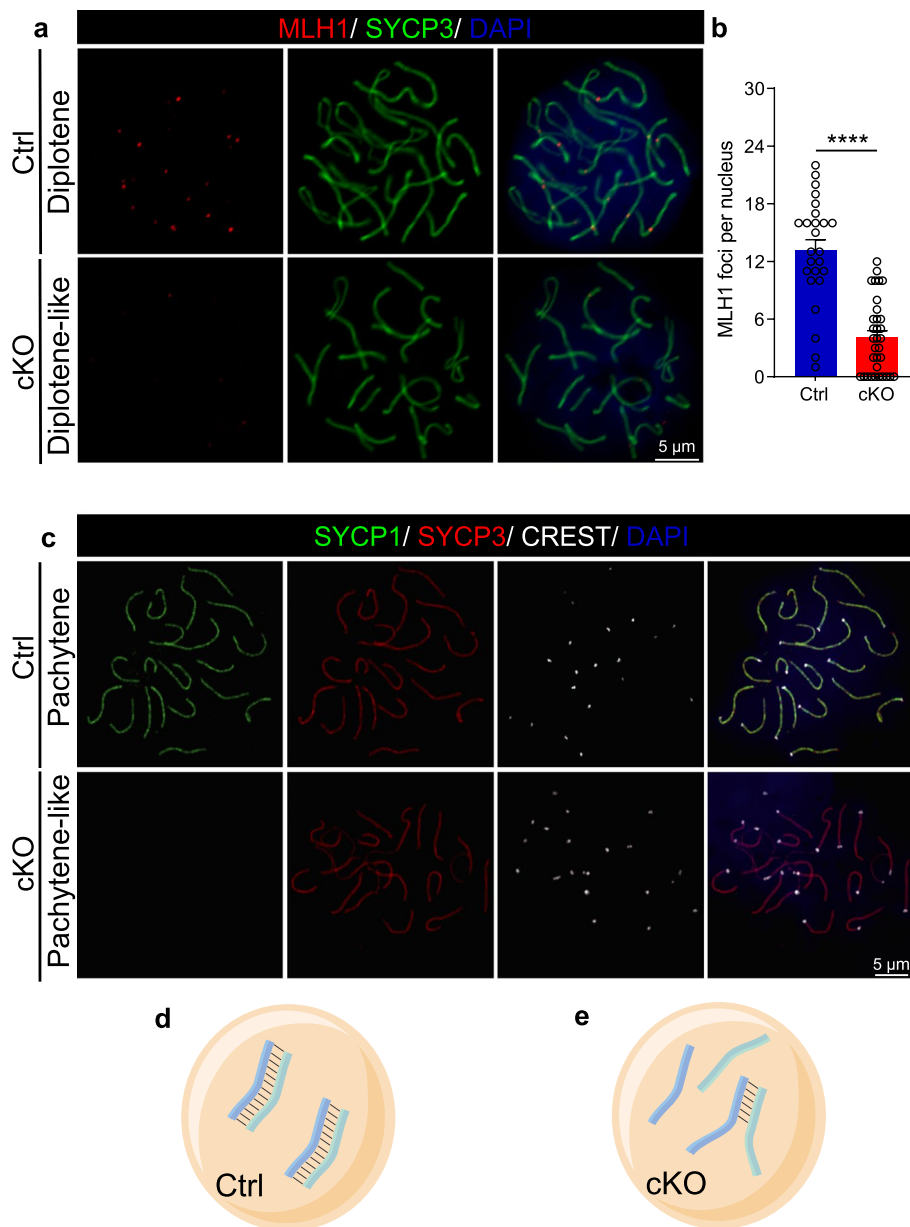
Page 10 of 18

Fig. 5 SRSF1 deficiency impairs chromosome synapsis and the formation of COs at meiotic prophase I. **a** Co-immunostaining of MLH1 and SYCP3 in newborn Ctrl and cKO oocytes. DNA was stained with DAPI. Scale bar, 5 μm. **b** The number of COs, marked by MLH1 foci (red), was significantly reduced in cKO diplotene-like oocytes compared with Ctrl oocytes. Twenty-five Ctrl oocytes and thirty-three cKO oocytes were obtained from 3 animals. Significance was determined by unpaired Student's *t* test; ****$P < 0.0001$. The error bar represents the mean ± SEM. **c** Localization of SYCP1, SYCP3, and CREST in newborn Ctrl and cKO oocytes. DNA was stained with DAPI. Scale bar, 5 μm. Diagrams illustrate aberrant synapsis in Ctrl (**d**) and cKO (**e**) oocytes

respectively, suggesting less effective DNA damage repair despite an increased number of DMC1 foci (Fig. 6a–f). Additionally, we found that low expression of the MSH5 protein led to defects in HR and synapsis (Fig. 7g, i, j). Defective oocytes with both persistent DNA damage and chromosome asynapsis may be eliminated by the combined effects of the synapsis and DNA damage

checkpoints. This study showed that defective oocytes were eliminated by this mechanism in the ovaries of newborn, 5 dpp, and adult mice (Figs. 2v and 3e, o). Interestingly, oocytes in meiotic arrest were detected in 5 dpp cKO mouse ovaries (Fig. 4g). The primordial follicle pool is depleted in 6 dpp $Msh5^{-/-}$ and $Six6os1^{-/-}$ mouse ovaries [62, 66]. Therefore, this is a significant reason that

Sun *et al. BMC Biology*   (2023) 21:49

Page 11 of 18

SRSF1 deficiency impairs quality control mechanisms. However, we could not illuminate the specific mechanism due to the premature deletion of SRSF1. Next, we will further develop this exciting work in other mouse models. Nevertheless, it is clear that SRSF1 is indispensable for oocyte survival.

In summary, our study provides an important theoretical basis for understanding the mechanisms of posttranscriptional regulation of oocyte meiosis by pre-mRNA splicing. Additionally, the discovery of the AS of POI-related genes in a mouse model provides the molecular basis for the clinical diagnosis and treatment of POI and the generation of eggs from induced stem cells.

Conclusions

This study demonstrates that SRSF1 plays a critical role in posttranscriptional regulation by specifically regulating the splicing of the POI-related genes *Msh5* and *Six6os1* during meiotic prophase I in mouse oocytes. This SRSF1-mediated posttranscriptional regulation is essential for primordial follicle formation and number determination (Fig. 8).

Methods

Mouse strains

C57BL/6N and ICR mice were purchased from Beijing Vital River Laboratory Animal Technology Co., Ltd. *Srsf1^{Fl/Fl}* mice were generated in the laboratory of Prof. Xiangdong Fu (University of California, San Diego, USA) and were kindly provided by Prof. Yuanchao Xue (Institute of Biophysics, Chinese Academy of Sciences, Beijing, China) [29]. *Stra8-GFPCre* mice were kindly provided by Prof. Minghan Tong (Shanghai Institute of Biochemistry and Cell Biology, Chinese Academy of Sciences, Shanghai, China) [35, 36]. To generate *Srsf1* cKO mice, *Stra8-GFPCre* mice were crossed with *Srsf1^{Fl/Fl}* mice. The primers used for PCR to genotype *Srsf1^{Fl/Fl}* and *Stra8-GFPCre* mice are shown in Additional file 6: Table 3. All mice were bred and housed under specific pathogen-free conditions with controlled temperature (22 ± 1 °C) and exposed to a constant 12-h light–dark cycle in the animal facilities of China Agricultural University. All experiments were conducted according to the guidelines and with the approval of the Institutional Animal Care and Use Committee of China Agricultural University (No. AW80401202-3–6).

Fertility test

For 3 months, two 6-week-old female mice were caged with one 8-week-old C57BL/6N male wild-type mouse. The number of pups from each female was recorded each day, and the date of parturition was recorded. These results were used to analyse the reproductive curve.

Immunostaining and histologic analysis

Mouse ovaries were fixed with 4% paraformaldehyde (P6148-500G, Sigma–Aldrich, Missouri, USA) in PBS (pH 7.4) at 4 °C overnight, dehydrated in graded ethanol solutions, vitrified with xylene, and embedded in paraffin. Tissue sections were cut at a 5-μm thickness for immunostaining and histologic analysis or an 8-μm thickness for counting the follicles in adult ovaries. For histological analysis, sections were dewaxed in xylene and rehydrated in graded ethanol solution and then stained with haematoxylin. After sealing the slides with neutral resin, a Ventana DP200 system was used for imaging. For immunofluorescence analysis, antigen retrieval was performed by microwaving the sections with sodium citrate buffer (pH 6.0). After blocking with 10% goat serum at room temperature for 1 h, the sections were incubated with primary antibodies in 5% goat serum (Additional file 7: Table 4) overnight at 4 °C. After washing with PBS, the sections were incubated with secondary antibodies (Additional file 7: Table 4) at room temperature in the dark for 1 h. The slides were mounted in antifade mounting medium with DAPI (P0131, Beyotime, Shanghai, China). Photos were taken with a Nikon A1 laser scanning confocal microscope and a Zeiss OPTOME fluorescence microscope. For immunohistochemistry analysis, the same protocol that was applied for immunofluorescence analysis was followed up to the heat-mediated antigen retrieval step, and subsequent operations followed the IHC kit instructions (SP-9000, ZSGB-BIO, Beijing, China). Colour visualization in the sections was achieved with a DAB horseradish peroxidase colour development kit (ZLI-9017, ZSGB-BIO, Beijing, China). Imaging

(See figure on next page.)

Fig. 6 SRSF1 is necessary for the resection of DSBs. **a** Co-immunostaining of γH2AX and SYCP3 in 18.5 dpc Ctrl and cKO ovaries. DNA was stained with DAPI. Scale bar of the top panel, 50 μm. Scale bar of the rest panel, 10 μm. **b** Percentage of double-positive cells is shown as the mean ± SEM in 18.5 dpc ovaries. Ctrl, $n=6$; cKO, $n=5$. **c** Co-immunostaining of RPA1 and SYCP3 in newborn Ctrl and cKO oocytes. DNA was stained with DAPI. Scale bar, 5 μm. **d** In cKO diplotene-like oocytes, the number of RPA1 foci (red) was maintained at a relatively high level. Twenty-five Ctrl oocytes and thirty-three cKO oocytes were obtained from 3 animals. **e** Localization of DMC1, γH2AX, and SYCP3 in 18.5 dpc Ctrl and cKO oocytes. DNA was stained with DAPI. Scale bar, 10 μm. **f** In cKO pachytene oocytes, the number of DMC1 foci (white) was maintained at a relatively high level. Sixty Ctrl oocytes and fifty-six cKO oocytes were obtained from 4 animals. Significance was determined by unpaired Student's *t* test; detailed *P* value $P \geq 0.05$, *$P < 0.05$, ***$P < 0.001$, ****$P < 0.0001$. The error bar represents the mean ± SEM
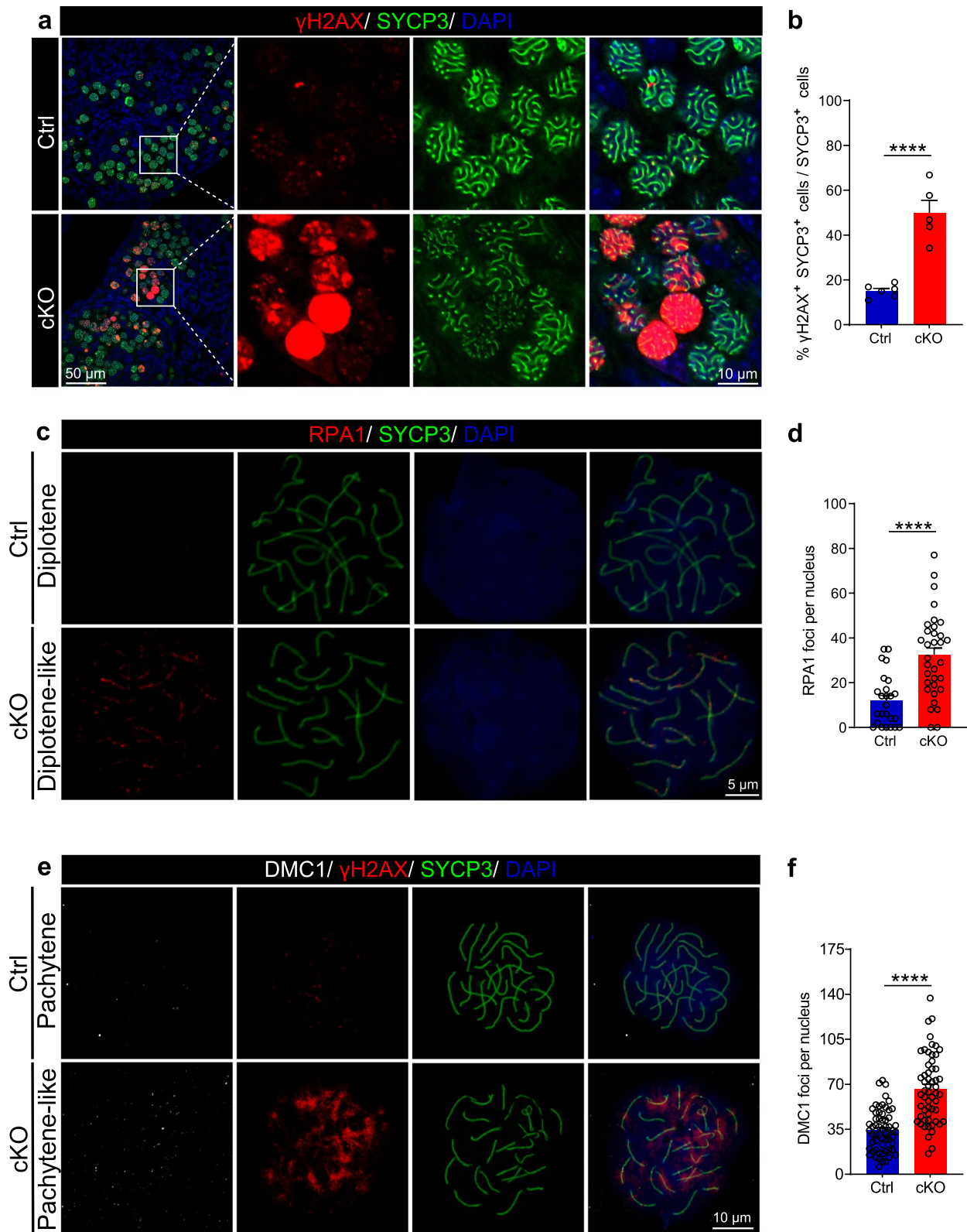
Sun *et al. BMC Biology*   (2023) 21:49

Page 12 of 18

Fig. 6 (See legend on previous page.)

Sun *et al. BMC Biology*   (2023) 21:49

Page 13 of 18

was performed according to the histological analysis protocol.

Quantification of follicles and oocytes
Serial 8-μm sections were cut from paraffin-embedded adult ovaries. All follicles or oocytes in VASA immunostained ovarian sections were counted. Follicle types were classified according to the following structural characteristics. As described previously [67], the following follicle types were distinguished: primordial follicles (type 1 and type 2), primary follicles (type 3), secondary follicles (type 4 and type 5), and antral follicles (types 6 − 8).

Serial 5-μm sections were obtained from paraffin-embedded ovaries from 5 dpp and newborn mice. The sections were stained with haematoxylin, and the following categories of oocytes and follicles were counted in every fifth section: primordial follicles (oocytes approximately 20 μm in diameter surrounded by 3 − 5 flat pregranulosa cells each); oocytes in cysts (two or more oocytes with shared cytoplasm); and naked oocytes (oocytes without any granulosa cells). As described previously [68], the sum of these counts was multiplied by five to estimate the total number of oocytes and follicles in each ovary.

Oocyte surface spreading
Oocyte purification was performed as described previously [69]. In brief, mouse ovaries were isolated and digested with 90 μl of TrypLE (12,604,021, Thermo, New York, US) at 37 °C for 10 min under constant shock. Digestion was terminated by adding 10 μl foetal bovine serum (C0235, Beyotime, Shanghai, China). After centrifugation at 1000 rpm for 1 min, the supernatant was discarded, and the cells were treated with 80 μl hypotonic buffer (30 mM Tris–HCl, 17 mM trisodium citrate dihydrate, 50 mM sucrose, 5 mM EDTA, 0.5 mM DTT, pH 8.2) containing proteinase inhibitor (1:100, P1005, Beyotime, Shanghai, China) for 30 min. Slides were pretreated with 20 μl of fixation buffer (1% paraformaldehyde, pH 9.2 with 50 mM boric acid) containing 0.15% Triton X-100 (T9284, Sigma, Missouri, USA) applied evenly on slides in advance. Then, 20 μl aliquots of the cell suspension were dripped onto the slides, which were incubated at 37 °C for 4 h in a humidified box. The samples were left to dry at room temperature. Then, immunofluorescence staining was performed according to the protocol described above.

RT–PCR and RT–qPCR
Total RNA was extracted by using RNAiso Plus (9109, Takara, Kusatsu, Japan) and a Direct-zol RNA Micro-Prep kit (R2060, Zymo Research, California, USA), and the concentration was measured with a Nano-300 ultramicro spectrophotometer (Allsheng, Hangzhou, China). cDNA was obtained according to the instructions of the TIANScript II RT kit (KR107, TIANGEN, Beijing, China). The expression of transcripts of the target gene was measured by using a Light Cycle® 96 instrument (Roche) with Hieff UNICON SYBR green master mix (11198ES08, Yeasen, Shanghai, China). AS analyses were performed on a RePure-A PCR instrument (BIO-GENER, Hangzhou,China). Primers were synthesized by Sangon Biotech (Additional file 6: Table 3). The expression level of *Gapdh* or *Vasa* was used as the control, and this value was set as 1. The relative transcript expression levels of other samples were obtained by comparing them with the control results.

RNA stability assay
One half of an ovary was treated with 50 μg/mL actinomycin D (ActD, SBR00013, Sigma–Aldrich, Missouri, USA) for transcription inhibition. Samples were collected at 0 and 120 min after transcription inhibition. The RNA stabilities of *Msh5* and *Six6os1* were determined by analysing total RNA without gDNA.

RNA-seq
Total RNA was extracted from mouse ovaries according to the above protocol at 16.5 dpc. Briefly, mRNA was purified from total RNA using poly-T oligo-attached

(See figure on next page.)

Fig. 7 SRSF1 directly regulates the splicing of *Msh5* and *Six6os1*. **a** Five AS events were significantly affected by SRSF1-deficient oocytes. rMATS (3.2.5) software was used to analyse AS events (FDR < 0.05). FDR, false discovery rate calculated from the *P* value. **b** Scatter plot of the GO enrichment analysis of the 191 affected AS events. **c** A schematic of the regulation of the splicing of *Msh5* and *Six6os1*. Integrative Genomics Viewer (IGV, version 2.10.2) was used to visualize and confirm AS events in RNA-seq data. E, exon. **d** The ectopic splicing of *Msh5* and *Six6os1* in cKO ovaries was analysed by RT–PCR (*n* = 4 per group). The scheme and cumulative data on the percentage of the indicated fragment are shown accordingly. **e, f** SRSF1 directly regulated the expression of *Msh5* and *Six6os1* by RIP–qPCR in 16.5 dpc mouse ovaries. *n* = 3. **g, h** Western blotting of MSH5 and SIX6OS1 expression in 17.5 dpc Ctrl and cKO ovaries. GAPDH (**g**) or ACTB (**h**) served as a loading control. *n* = 4. **i** Localization of MSH5 and SYCP3 in 17.5 dpc Ctrl and cKO oocytes. DNA was stained with DAPI. Scale bar, 10 μm. **j** The number of MSH5 foci (green) was significantly reduced in cKO pachytene oocytes compared with Ctrl oocytes. Sixty Ctrl oocytes and sixty cKO oocytes were obtained from 4 animals. **k** Co-immunostaining of SIX6OS1 and SYCP3 in 17.5 dpc Ctrl and cKO ovaries. DNA was stained with DAPI. Zyg, zygotene; ePac, early pachytene; Pac, pachytene. Scale bar, 10 μm. **l** The expression of *Six6os1* in 16.5 dpc cKO ovaries after ActD treatment at different times. *n* = 4. Significance was determined by unpaired Student's *t* test; detailed *P* value *P* ≥ 0.05, **P* < 0.05, ***P < 0.001, ****P < 0.0001. The error bar represents the mean ± SEM
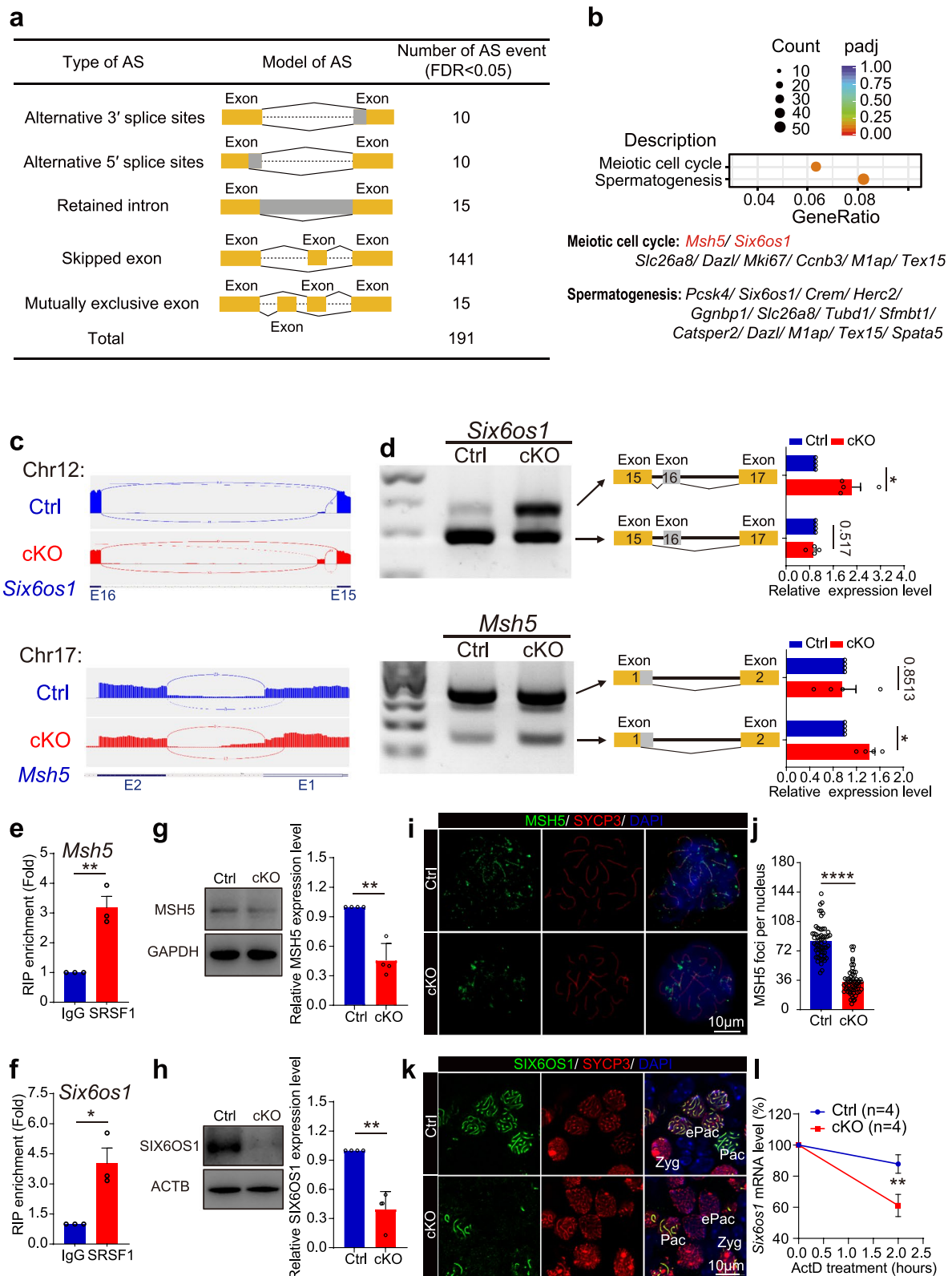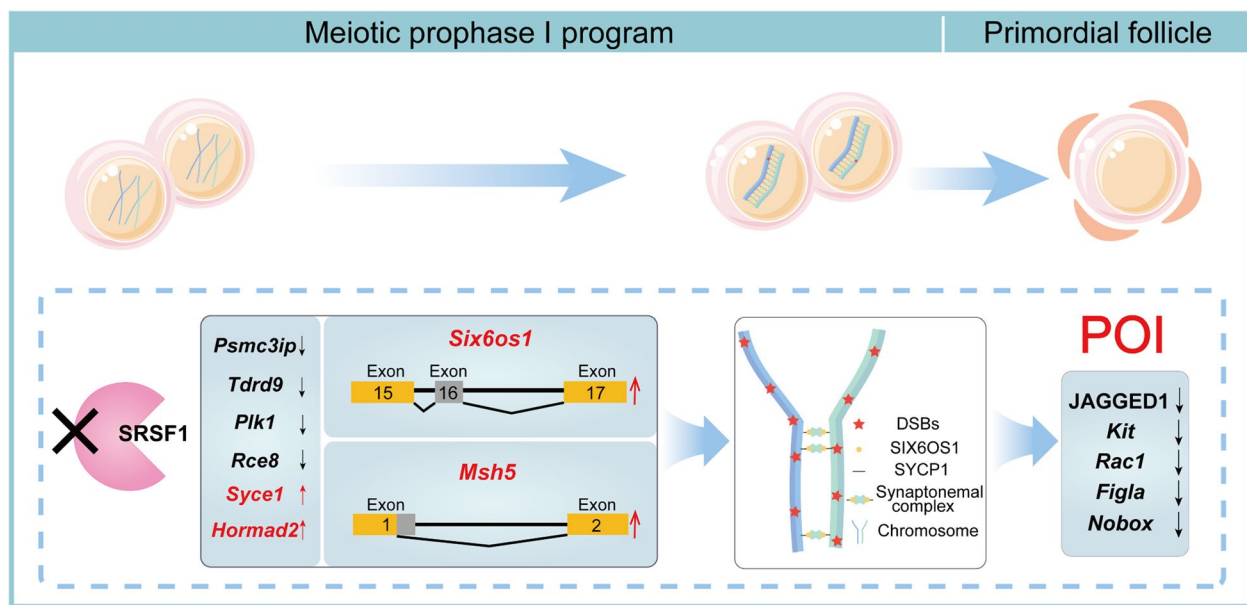
Fig. 7 (See legend on previous page.)

Fig. 8 A schematic illustration of the molecular mechanisms by which SRSF1 regulates primordial follicle formation and number determination during meiotic prophase I

magnetic beads. After fragmentation, we established a transcriptome sequencing library and assessed library quality on an Agilent Bioanalyzer 2100 system. The clustering of the index-coded samples was performed on a cBot Cluster Generation System using a TruSeq PE Cluster kit v3-cBot-HS (Illumina) according to the manufacturer's instructions. After cluster generation, the library preparations were sequenced on the Illumina NovaSeq platform, and 150 bp paired-end reads were generated. After quality control, all the downstream analyses were performed on clean, high-quality data. The index of the reference genome was built, and paired-end clean reads were aligned to the reference genome using HISAT2 software (version 2.0.5). FeatureCounts (version 1.5.0) was used to count the number of reads mapped to each gene. Then, the fragments per kilobase million (FPKM) value of each gene was calculated based on the length of the gene and the read count mapped to this gene. Differential expression analysis of cKO/Ctrl ovaries (three biological replicates per condition) was performed using the DESeq2 R package (version 1.20.0). Genes with a P value < 0.05 identified by DESeq2 were considered differentially expressed.

AS analysis

rMATS software (version 3.2.5) was used to analyse the AS events in cKO mouse ovaries based on RNA-seq data. Five types of AS events (SE, RI, MXE, A5SS, and A3SS) were revealed by rMATS software. Our threshold for screening differentially significant AS events was a false

discovery rate (FDR) less than 0.05. Splicing events with an FDR less than 0.05 and an inclusion-level difference with a significance of at least 5% (0.05) were considered statistically significant. The IGV (Version 2.10.2) was used to visualize and confirm AS events based on RNA-seq data.

GO term enrichment analysis

The GO enrichment analysis of differentially expressed genes and AS genes was implemented with the cluster-Profiler R package (version 3.4.4), in which gene length bias was corrected. Mouse genome data (GRCm38/mm10) were used as the reference, and Benjamini–Hochberg multiple tests were applied to adjust multiple testing. GO terms with corrected P values of less than 0.05 were considered significantly enriched by differentially expressed genes and AS genes.

Western blotting

Total protein was extracted with cell lysis buffer (P0013, Beyotime, Shanghai, China) containing PMSF (1:100, ST506, Beyotime, Shanghai, China) and a protease inhibitor cocktail (1:100, P1005, Beyotime, Shanghai, China). A BCA protein assay kit (CW0014S, CWBiotech, Beijing, China) was used to measure the protein concentration. The protein lysates were electrophoretically separated on sodium dodecyl sulfate–polyacrylamide gels and electrically transferred to polyvinylidene fluoride membranes (IPVH00010, Millipore, Ireland). The membranes were blocked in 5% skimmed milk for 1 h and incubated with

the primary antibodies (Additional file 7: Table 4) for one night at 4 °C. Then, the membranes were incubated with secondary antibodies (Additional file 7: Table 4) at room temperature for 1 h. Proteins were visualized using the Tanon 5200 chemiluminescence imaging system following incubation with BeyoECL Plus (P0018S, Beyotime, Shanghai, China).

RNA immunoprecipitation (RIP) and RIP–qPCR

As described previously [70], RIP was performed using 16.5 dpc mouse ovaries. The ovaries were lysed in cell lysis buffer (P0013, Beyotime, Shanghai, China) containing PMSF (1:100, ST506, Beyotime, Shanghai, China), a proteinase inhibitor cocktail (1:100, P1005, Beyotime, Shanghai, China), DTT (1:50, ST041-2 ml, Beyotime, Shanghai, China), and an RNase inhibitor (1:20, R0102-10 kU, Beyotime, Shanghai, China). After incubation on ice for 20 min, the lysate was added to 20 µl of protein A agarose (P2051-2 ml, Beyotime, Shanghai, China) for preclearing at 4 °C for 1 h. Two micrograms of an SRSF1 antibody (sc-33652, Santa Cruz Biotechnology, California, USA) and a normal mouse IgG (sc-3879, Santa Cruz Biotechnology, California, USA) were added to the lysate, followed by overnight incubation at 4 °C. The next day, 60 µl of protein A agarose was added to the lysate followed by incubation at 4 °C for 4 h. The agarose complexes containing antibodies, target proteins, and RNA were washed for 5 min at 4 °C, which was repeated 3 times. Protein-bound RNA was then extracted using RNAiso Plus and the Direct-zol RNA MicroPrep kit. RIP–qPCR was performed according to the above RT–qPCR protocol.

Statistical analysis

GraphPad Prism software (version 9.0.0) was used for the statistical analyses, and the values and error bars shown represent the mean ± SEM. Significant differences between the two groups were analysed using Student's t test. Statistical significance was considered as follows: detailed P value $P \geq 0.05$; *$P < 0.05$; **$P < 0.01$; ***$P < 0.001$; ****$P < 0.0001$).

Abbreviations

AS	Alternative splicing
SRSF1/SF2/ASF	Serine/arginine-rich splicing factor 1
cKO	Conditional knockout
POI	Primary ovarian insufficiency
LHX8	LIM homeobox protein 8
NOBOX	Newborn ovary homeobox protein
SOHLH	Spermatogenesis- and oogenesis-specific basic helix-loop-helix-containing protein
FIGLA	Factor in the germline alpha
JAG1	Protein jagged-1
RAC1	Ras-related C3 botulinum toxin substrate 1
STRA8	Stimulated by retinoic acid gene 8 protein
COs	DNA crossovers
DSB	SPO11-linked DNA double-strand break
NGS	Next-generation sequencing
SC	Synaptonemal complex
STAG3	Stromal antigen 3
SMC	Structural maintenance of chromosomes
SYCE	Synaptonemal complex central element
C14ORF39/SIX6OS1	Six6 opposite strand transcript 1 homologue
TEX12	Testis-expressed protein 12
MEIOB	Meiosis-specific with OB domain-containing protein
MCM	Mini-chromosome maintenance
MSH	MutS protein homologue
SYCP	Synaptonemal complex protein
dpc	Days post-coitus
dpp	Days post-partum
RT	Reverse transcription
qPCR	Quantitative real-time PCR
GM130	130 KDa cis-Golgi matrix protein
Ctrl	Control
GO	Gene Ontology
TDRD9	Tudor domain-containing protein 9
PLK1	Polo-like kinase 1
HORMAD2	HORMA domain-containing protein 2
MSY2	Germ cell-specific Y-box-binding protein
MLH1	MutL homologue 1
HR	Homologous recombination
γH2AX	Phosphorylated histone H2AX
RPA	Replication protein A
FDR	False discovery rate calculated from the P value
SEs	Skipped exons
A5SSs	Alternative 5′ splice sites
A3SSs	Alternative 3′ splice sites
MXEs	Mutually exclusive exons
RIs	Retained introns
IGV	Integrative Genomics Viewer
RIP	RNA immunoprecipitation
SPIDR	Scaffolding protein involved in DNA repair
IRF7	Interferon regulatory factor 7
IL27RA	Interleukin-27 receptor subunit alpha
MYO1B	Myosin IB
ICR	Institute of Cancer Research
GAPDH	Glyceraldehyde-3-phosphate dehydrogenase
ActD	Actinomycin D

Supplementary Information

Additional file 1: Fig. S1. The expression pattern of SRSF1 in ovarian development and ageing. a The expression of *Srsf1* during ovarian development and ageing. Real-time qPCR data were normalized to *Gapdh*. b Western blotting of SRSF1 expression in 17.5 dpc Ctrl and cKO ovaries. c The relative protein expression level of SRSF1 is shown in ovarian development and ageing. ACTB served as a loading control. The value in 12 M ovaries was set as 1.0. d Immunostaining was performed using VASA and SRSF1 antibodies from NB, 6 W, and 10 M ovaries. DNA was stained with DAPI. Scale bar, 10 μm. NB, newborn; W, week; M, month.

Additional file 2: Table 1. Differential genes were analysed in this study.

Additional file 3: Table 2. AS events were analysed in cKO and Ctrl ovaries.

Additional file 4: Fig. S2. SRSF1 regulates the stability of *Msh5* and *Six6os1*. a, b Western blotting of MSH5 and SIX6OS1 expression in 17.5 dpc Ctrl and cKO ovaries. GAPDH (a) or ACTB (b) served as a loading control. c The expression of *Msh5* in 16.5 dpc cKO ovaries after ActD treatment at different times. *n*=4.

Additional file 5: Fig. S3. Various genes were visually analysed using IGV.

Additional file 6: Table 3. Primer sequences were used in this study.

Sun *et al. BMC Biology*   (2023) 21:49

Page 17 of 18

Additional file 7: Table 4. Antibodies were used in this study.

Additional file 8. Uncropped gels/blots.

Additional file 9. Individual data values.

Availability of data and materials
All data generated or analysed during this study are included in this published article, its supplementary information files and publicly available repositories. The uncropped gels/blots are provided in Additional file 8. The individual data values for Figs. 2, 3, 4, 5, 6, and 7, as well as Additional file 1: Fig. S1 and Additional file 4: Fig. S2, are provided in Additional file 9. The RNA-seq data were deposited in GEO (https://www.ncbi.nlm.nih.gov/geo/) under accession number GSE198205.

Declarations

Ethics approval and consent to participate
All experiments were conducted following the guidelines and with the approval of the Institutional Animal Care and Use Committee of China Agricultural University (No. AW80401202-3–6).

Consent for publication
Not applicable.

Competing interests
The authors declare that they have no completing interests.

References
1. Qiao HY, Rao HBDP, Yun Y, Sandhu S, Fong JH, Sapre M, et al. Impeding DNA break repair enables oocyte quality control. Mol Cell. 2018;72(2):211–21.
2. Edson MA, Nagaraja AK, Matzuk MM. The mammalian ovary from genesis to revelation. Endocr Rev. 2009;30(6):624–712.
3. Broekmans FJ, Knauff EAH, Velde ERT, Macklon NS, Fauser BC. Female reproductive ageing: current knowledge and future trends. Trends Endocrinol Metab. 2007;18(2):58–65.
4. Ellnati E, Zielinska AP, McCarthy A, Kubikova N, Maciulyte V, Mahadevaiah S, et al. The BCL-2 pathway preserves mammalian genome integrity by eliminating recombination-defective oocytes. Nat Commun. 2020;11(1):2598.
5. Jiao X, Ke H, Qin Y, Chen ZJ. Molecular genetics of premature ovarian insufficiency. Trends Endocrinol Metab. 2018;29(11):795–807.
6. Huang CZ, Guo T, Qin YY. Meiotic recombination defects and premature ovarian insufficiency. Front Cell Dev Biol. 2021;9:652407.
7. Franca MM, Mendonca BB. Genetics of ovarian insufficiency and defects of folliculogenesis. Best Pract Res Clin Endocrinol Metab. 2022;36(1):101594.
8. Ishiguro KI. The cohesin complex in mammalian meiosis. Genes Cells. 2019;24(1):6–30.
9. Mellone S, Zavattaro M, Vurchio D, Ronzani S, Caputo M, Leone I, et al. A long contiguous stretch of homozygosity disclosed a novel STAG3 biallelic pathogenic variant causing primary ovarian insufficiency: a case report and review of the literature. Genes (Basel). 2021;12(11):1709.
10. Jaillard S, McElreavy K, Robevska G, Akloul L, Ghieh F, Sreenivasan R, et al. STAG3 homozygous missense variant causes primary ovarian insufficiency and male non-obstructive azoospermia. Mol Hum Reprod. 2020;26(9):665–77.
11. Caburet S, Arboleda VA, Llano E, Overbeek PA, Barbero JL, Oka K, et al. Mutant cohesin in premature ovarian failure. N Engl J Med. 2014;370(10):943–9.
12. Franca MM, Nishi MY, Funari MFA, Lerario AM, Baracat EC, Hayashida SAY, et al. Two rare loss-of-function variants in the STAG3 gene leading to primary ovarian insufficiency. Eur J Med Genet. 2019;62(3):186–9.
13. Heddar A, Dessen P, Flatters D, Misrahi M. Novel STAG3 mutations in a Caucasian family with primary ovarian insufficiency. Mol Genet Genomics. 2019;294(6):1527–34.
14. Colombo R, Pontoglio A, Bini M. A STAG3 missense mutation in two sisters with primary ovarian insufficiency. Eur J Obstet Gynecol Reprod Biol. 2017;216:269–71.
15. He WB, Banerjee S, Meng LL, Du J, Gong F, Huang H, et al. Whole-exome sequencing identifies a homozygous donor splice-site mutation in STAG3 that causes primary ovarian insufficiency. Clin Genet. 2018;93(2):340–4.
16. Le Quesne SP, Williams HJ, James C, Tekman M, Stanescu HC, Kleta R, et al. STAG3 truncating variant as the cause of primary ovarian insufficiency. Eur J Hum Genet. 2016;24(1):135–8.
17. Xiao WJ, He WB, Zhang YX, Meng LL, Lu GX, Lin G, et al. In-frame variants in STAG3 gene cause premature ovarian insufficiency. Front Genet. 2019;10:1016.
18. Demain LAM, Boetje E, Edgerley JJ, Miles E, Fitzgerald CT, Busby G, et al. Biallelic loss of function variants in STAG3 result in primary ovarian insufficiency. Reprod Biomed Online. 2021;43(5):899–902.
19. Sanchez-Saez F, Gomez HL, Dunne OM, Gallego-Paramo C, Felipe-Medina N, Sanchez-Martin M, et al. Meiotic chromosome synapsis depends on multivalent SYCE1-SIX6OS1 interactions that are disrupted in cases of human infertility. Sci Adv. 2020;6(36):eabb1660.
20. Fan S, Jiao Y, Khan R, Jiang X, Javed AR, Ali A, et al. Homozygous mutations in C14orf39/SIX6OS1 cause non-obstructive azoospermia and premature ovarian insufficiency in humans. Am J Hum Genet. 2021;108(2):324–36.
21. Zhe J, Ye D, Chen X, Liu Y, Zhou X, Li Y, et al. Consanguineous Chinese familial study reveals that a gross deletion that includes the SYCE1 gene region is associated with premature ovarian insufficiency. Reprod Sci. 2020;27(2):461–7.
22. de Vries L, Behar DM, Smirin-Yosef P, Lagovsky I, Tzur S, Basel-Vanagaite L. Exome sequencing reveals SYCE1 mutation associated with autosomal recessive primary ovarian insufficiency. J Clin Endocrinol Metab. 2014;99(10):E2129–32.
23. McGuire MM, Bowden W, Engel NJ, Ahn HW, Kovanci E, Rajkovic A. Genomic analysis using high-resolution single-nucleotide polymorphism arrays reveals novel microdeletions associated with premature ovarian failure. Fertil Steril. 2011;95(5):1595–600.
24. Caburet S, Todeschini AL, Petrillo C, Martini E, Farran ND, Legois B, et al. A truncating MEIOB mutation responsible for familial primary ovarian insufficiency abolishes its interaction with its partner SPATA22 and their recruitment to DNA double-strand breaks. EBioMedicine. 2019;42:524–31.

Sun *et al. BMC Biology* (2023) 21:49

Page 18 of 18

25. Carlosama C, Elzaiat M, Patino LC, Mateus HE, Veitia RA, Laissue P. A homozygous donor splice-site mutation in the meiotic gene MSH4 causes primary ovarian insufficiency. Hum Mol Genet. 2017;26(16):3161–6.

26. Wood-Trageser MA, Gurbuz F, Yatsenko SA, Jeffries EP, Kotan LD, Surti U, et al. MCM9 mutations are associated with ovarian failure, short stature, and chromosomal instability. Am J Hum Genet. 2014;95(6):754–62.

27. Das S, Krainer AR. Emerging functions of SRSF1, splicing factor and oncoprotein, in RNA metabolism and cancer. Mol Cancer Res. 2014;12(9):1195–204.

28. Paz S, Ritchie A, Mauer C, Caputi M. The RNA binding protein SRSF1 is a master switch of gene expression and regulation in the immune system. Cytokine Growth Factor Rev. 2021;57:19–26.

29. Xu X, Yang D, Ding JH, Wang W, Chu PH, Dalton ND, et al. ASF/SF2-regulated CaMKIIdelta alternative splicing temporally reprograms excitation-contraction coupling in cardiac muscle. Cell. 2005;120(1):59–72.

30. Qi Z, Wang F, Yu G, Wang D, Yao Y, You M, et al. SRSF1 serves as a critical posttranscriptional regulator at the late stage of thymocyte development. Sci Adv. 2021;7(16):eabf0753.

31. Liu J, You M, Yao Y, Ji C, Wang Z, Wang F, et al. SRSF1 plays a critical role in invariant natural killer T cell development and function. Cell Mol Immunol. 2021;18(11):2502–15.

32. Katsuyama T, Moulton VR. Splicing factor SRSF1 is indispensable for regulatory T cell homeostasis and function. Cell Rep. 2021;36(1):109339.

33. Katsuyama T, Li H, Comte D, Tsokos GC, Moulton VR. Splicing factor SRSF1 controls T cell hyperactivity and systemic autoimmunity. J Clin Invest. 2019;129(12):5411–23.

34. Niu W, Spradling AC. Two distinct pathways of pregranulosa cell differentiation support follicle formation in the mouse ovary. Proc Natl Acad Sci U S A. 2020;117(33):20015–26.

35. Lin Z, Hsu PJ, Xing X, Fang J, Lu Z, Zou Q, et al. Mettl3-/Mettl14-mediated mRNA N(6)-methyladenosine modulates murine spermatogenesis. Cell Res. 2017;27(10):1216–30.

36. Chen Y, Zheng Y, Gao Y, Lin Z, Yang S, Wang T, et al. Single-cell RNA-seq uncovers dynamic processes and critical regulators in mouse spermatogenesis. Cell Res. 2018;28(9):879–96.

37. Lei L, Spradling AC. Mouse oocytes differentiate through organelle enrichment from sister cyst germ cells. Science. 2016;352(6281):95–9.

38. Wang Z, Liu CY, Zhao Y, Dean J. FIGLA, LHX8 and SOHLH1 transcription factor networks regulate mouse oocyte growth and differentiation. Nucleic Acids Res. 2020;48(7):3525–41.

39. Wang Y, Teng Z, Li G, Mu X, Wang Z, Feng L, et al. Cyclic AMP in oocytes controls meiotic prophase I and primordial folliculogenesis in the perinatal mouse ovary. Development. 2015;142(2):343–51.

40. Hunter N. Meiotic recombination: the essence of heredity. Cold Spring Harb Perspect Biol. 2015;7(12):a016618.

41. Shang Y, Huang T, Liu H, Liu Y, Liang H, Yu X, et al. MEIOK21: a new component of meiotic recombination bridges required for spermatogenesis. Nucleic Acids Res. 2020;48(12):6624–39.

42. Guan Y, Leu NA, Ma J, Chmatal L, Ruthel G, Bloom JC, et al. SKP1 drives the prophase I to metaphase I transition during male meiosis. Sci Adv. 2020;6(13):eaaz2129.

43. Grive KJ, Gustafson EA, Seymour KA, Baddoo M, Schorl C, Golnoski K, et al. TAF4b regulates oocyte-specific genes essential for meiosis. Plos Genet. 2016;12(6):e1006128.

44. Gray S, Cohen PE. Control of meiotic crossovers: from double-strand break formation to designation. Annu Rev Genet. 2016;50:175–210.

45. Qu W, Liu C, Xu YT, Xu YM, Luo MC. The formation and repair of DNA double-strand breaks in mammalian meiosis. Asian J Androl. 2021;23(6):572–9.

46. Mahadevaiah SK, Turner JM, Baudat F, Rogakou EP, de Boer P, Blanco-Rodriguez J, et al. Recombinational DNA double-strand breaks in mice precede synapsis. Nat Genet. 2001;27(3):271–6.

47. Shi B, Xue J, Yin H, Guo R, Luo M, Ye L, et al. Dual functions for the ssDNA-binding protein RPA in meiotic recombination. Plos Genet. 2019;15(2):e1007952.

48. Guo T, Zhao S, Zhao S, Chen M, Li G, Jiao X, et al. Mutations in MSH5 in primary ovarian insufficiency. Hum Mol Genet. 2017;26(8):1452–7.

49. Wang C, Zhou B, Xia G. Mechanisms controlling germline cyst breakdown and primordial follicle formation. Cell Mol Life Sci. 2017;74(14):2547–66.

50. Choi Y, Ballow DJ, Xin Y, Rajkovic A. Lim homeobox gene, lhx8, is essential for mouse oocyte differentiation and survival. Biol Reprod. 2008;79(3):442–9.

51. Rajkovic A, Pangas SA, Ballow D, Suzumori N, Matzuk MM. NOBOX deficiency disrupts early folliculogenesis and oocyte-specific gene expression. Science. 2004;305(5687):1157–9.

52. Pangas SA, Choi Y, Ballow DJ, Zhao Y, Westphal H, Matzuk MM, et al. Oogenesis requires germ cell-specific transcriptional regulators Sohlh1 and Lhx8. Proc Natl Acad Sci U S A. 2006;103(21):8090–5.

53. Soyal SM, Amleh A, Dean J. FIG alpha, a germ cell-specific transcription factor required for ovarian follicle formation. Development. 2000;127(21):4645–54.

54. Jones RL, Pepling ME. KIT signaling regulates primordial follicle formation in the neonatal mouse ovary. Dev Biol. 2013;382(1):186–97.

55. Vanorny DA, Prasasya RD, Chalpe AJ, Kilen SM, Mayo KE. Notch signaling regulates ovarian follicle formation and coordinates follicular growth. Mol Endocrinol. 2014;28(4):499–511.

56. Zhao L, Du X, Huang K, Zhang T, Teng Z, Niu W, et al. Rac1 modulates the formation of primordial follicles by facilitating STAT3-directed Jagged1, GDF9 and BMP15 transcription in mice. Sci Rep. 2016;6:23972.

57. Stringer JM, Winship A, Zerafa N, Wakefield M, Hutt K. Oocytes can efficiently repair DNA double-strand breaks to restore genetic integrity and protect offspring health. Proc Natl Acad Sci U S A. 2020;117(21):11513–22.

58. Zhou X, Wang R, Li X, Yu L, Hua D, Sun C, et al. Splicing factor SRSF1 promotes gliomagenesis via oncogenic splice-switching of MYO1B. J Clin Invest. 2019;129(2):676–93.

59. Snowden T, Acharya S, Butz C, Berardini M, Fishel R. hMSH4-hMSH5 recognizes Holliday Junctions and forms a meiosis-specific sliding clamp that embraces homologous chromosomes. Mol Cell. 2004;15(3):437–51.

60. Kneitz B, Cohen PE, Avdievich E, Zhu LY, Kane MF, Hou H, et al. MutS homolog 4 localization to meiotic chromosomes is required for chromosome pairing during meiosis in male and female mice. Gene Dev. 2000;14(9):1085–97.

61. de Vries SS, Baart EB, Dekker M, Siezen A, de Rooij DG, de Boer P, et al. Mouse MutS-like protein Msh5 is required for proper chromosome synapsis in male and female meiosis. Genes Dev. 1999;13(5):523–31.

62. Gomez HL, Felipe-Medina N, Sanchez-Martin M, Davies OR, Ramos I, Garcia-Tunon I, et al. C14ORF39/SIX6OS1 is a constituent of the synaptonemal complex and is essential for mouse fertility. Nat Commun. 2016;7:13298.

63. Zickler D, Kleckner N. Recombination, pairing, and synapsis of homologs during meiosis. Cold Spring Harb Perspect Biol. 2015;7(6):a016626.

64. Kerr JB, Myers M, Anderson RA. The dynamics of the primordial follicle reserve. Reproduction. 2013;146(6):R205–15.

65. Klinger FG, Rossi V, De Felici M. Multifaceted programmed cell death in the mammalian fetal ovary. Int J Dev Biol. 2015;59(1–3):51–4.

66. Edelmann W, Cohen PE, Kneitz B, Winand N, Lia M, Heyer J, et al. Mammalian MutS homologue 5 is required for chromosome pairing in meiosis. Nat Genet. 1999;21(1):123–7.

67. Pedersen T, Peters H. Proposal for a classification of oocytes and follicles in the mouse ovary. J Reprod Fertil. 1968;17(3):555–7.

68. Flaws JA, Hirshfield AN, Hewitt JA, Babus JK, Furth PA. Effect of bcl-2 on the primordial follicle endowment in the mouse ovary. Biol Reprod. 2001;64(4):1153–9.

69. Peters AH, Plug AW, van Vugt MJ, de Boer P. A drying-down technique for the spreading of mammalian meiocytes from the male and female germline. Chromosome Res. 1997;5(1):66–8.

70. Gagliardi M, Matarazzo MRRIP. RNA immunoprecipitation. Methods Mol Biol. 2016;1480:73–86.

Publisher's Note